Endothelial deletion of hypoxia-inducible factor–2α (HIF-2α) alters vascular function and tumor angiogenesis

*Nicolas Skuli,[1,2] *Liping Liu,[1,2] Anja Runge,[1,2] Tao Wang,[3] Lijun Yuan,[3] Sunny Patel,[1] Luisa Iruela-Arispe,[4] M. Celeste Simon,[1,2,5] and Brian Keith[1-6]

[1]Abramson Family Cancer Research Institute, [2]Howard Hughes Medical Institute, and [3]Penn Cardiovascular Institute, University of Pennsylvania, Philadelphia; [4]Department of Molecular, Cell and Developmental Biology, University of California Los Angeles; and Departments of [5]Cell and Developmental Biology and [6]Cancer Biology, University of Pennsylvania School of Medicine, Philadelphia

Hypoxia-inducible factor–2α (HIF-2α) is highly expressed in embryonic vascular endothelial cells (ECs) and activates the expression of target genes whose products modulate vascular function and angiogenesis. In this report, we describe a genetic model designed to test the physiologic consequences of deleting HIF-2α in murine endothelial cells. Surprisingly, mice with HIF-2α–deficient ECs developed normally but displayed a variety of phenotypes, including increased vessel permeability, aberrant endothelial cell ultrastructure, and pulmonary hypertension. Moreover, these animals exhibited defective tumor angiogenesis associated with increased hypoxic stress and tumor cell apoptosis. Immortalized HIF-2α–deficient ECs displayed decreased adhesion to extracellular matrix proteins and expressed reduced levels of transcripts encoding fibronectin, integrins, endothelin B receptor, angiopoietin 2, and delta-like ligand 4 (Dll4). Together, these data identify unique cell-autonomous functions for HIF-2α in vascular endothelial cells. (Blood. 2009; 114:469-477)

Introduction

The generation and function of vascular endothelial cells (ECs), as well as the recruitment of support cells such as pericytes and vascular smooth muscle cells, is regulated by local physiologic stimuli.[1] In particular, the synthesis and activity of many angiogenic factors, including vascular endothelial growth factor (VEGF), the angiopoietins (Ang1-4), and their cognate receptors,[2] are modulated by the effects of infiltrating macrophages, extracellular matrix proteolysis, and tissue hypoxia (O_2 deprivation).[3,4] Of note, localized hypoxia regulates angiogenic responses during normal embryonic development and in pathophysiologic contexts such as solid tumor growth.[5,6]

Cells respond to hypoxia through multiple mechanisms, including the stabilization of hypoxia inducible factors (HIFs), which are heterodimeric bHLH-PAS transcriptional activators consisting of a distinct HIF-α subunit and HIF-β subunit (also called ARNT). HIFs stimulate the expression of more than 150 genes whose products orchestrate adaptive responses including angiogenesis, altered cellular metabolism, and increased erythropoiesis.[7,8] HIF activity is regulated primarily through hypoxia-induced posttranslational stabilization and activation of HIF-α subunits, reviewed in detail elsewhere.[9] The majority of HIF transcriptional activity is mediated by 2 distinct complexes consisting of ARNT bound to either of the highly related proteins HIF-1α or HIF-2α (also called EPAS-1/HRF/HLF/MOP2), which display a high degree of sequence similarity in critical functional domains.[8] Whereas HIF-1α appears to be expressed in most cell types, HIF-2α mRNA expression is detected most prominently in embryonic vascular ECs, kidney mesangial cells, neural crest-derived sympathetic ganglia, and epithelial cells of the developing lung.[10-13] Although HIF-1α and HIF-2α have partly overlapping sets of target genes, mounting evidence indicates that both proteins activate a distinct subset of hypoxically induced genes.[14,15] These data support the idea that HIF-1α and HIF-2α play unique and, in some cases, opposing roles in important cellular processes.[16,17]

The expression of HIF-2α in vascular ECs, along with its ability to regulate the expression of VEGF, VEGF receptor-1 (Flt-1), VEGF receptor-2 (Flk-1), and Tie2 (the receptor tyrosine kinase for angiopoietin, Ang1 and Ang2), suggests that HIF-2α plays an important role in angiogenesis. Obtaining in vivo support for this hypothesis has been confounded, however, by the complex phenotypes observed in 3 independent germ line murine HIF-2α knockout (KO) strains. Targeted HIF-2α deficiency results in embryonic or perinatal lethality associated with bradycardia, defective lung maturation, and mitochondrial dysfunction, depending on genetic background.[10,18-20] In one report, however, approximately 50% of HIF-2α–deficient embryos displayed yolk sac and embryonic vascular remodeling defects.[20] This vascular defect correlated to decreased Tie2 expression and was partly rescued by transgenic expression of a *Hif-2α* cDNA under the control of the *Tie2* promoter in some homozygous mutant embryos.[21] These data indicate that HIF-2α plays a functional role in murine ECs, although the precise mechanisms involved remained unclear.

To further investigate the role of HIF-2α in EC functions while circumventing the complex and various phenotypes observed in global *Hif-2α* deletion strains, we ablated HIF-2α function specifically in murine vascular ECs. These mice display specific defects in vessel integrity and tumor angiogenesis associated with decreased expression of fibronectin, integrins, endothelin B receptor (ET-B), Ang2, and delta-like ligand

Submitted December 8, 2008; accepted April 28, 2009. Prepublished online as *Blood* First Edition paper, May 13, 2009; DOI 10.1182/blood-2008-12-193581.

*N.S. and L.L. contributed equally to this work.

The online version of this article contains a data supplement.

The publication costs of this article were defrayed in part by page charge payment. Therefore, and solely to indicate this fact, this article is hereby marked "advertisement" in accordance with 18 USC section 1734.

4 (Dll4) in ECs. Collectively, these data establish a unique cell-autonomous role for HIF-2α in adult murine ECs.

Methods

Materials

Lewis lung carcinoma, murine endothelial MS1, and B16F1 and B16F10 melanoma cells were obtained from ATCC. Hypoxyprobe (pimonidazole) and corresponding antibody were obtained from Millipore and Apo-BrdU TUNEL assay kit from MBL International. ABC Elite and MOM kits were from Vector laboratories. Antibodies, used for immunohistochemistry, immunofluorescence, and Western blot analysis, were obtained from commercial suppliers (see supplemental information, available on the *Blood* website; see the Supplemental Materials link at the top of the online article).

Generation of conditional HIF-2α VE-cadherin-Cre mice

To delete HIF-2α function in ECs, mice carrying the conditional *Hif-2α*^{fl} allele[22] (supplemental Figure 1A-B) and were bred to transgenic mice expressing Cre recombinase under the VE-cadherin promoter (Cre)[23] to obtain experimental *Hif-2α*$^{fl/\Delta}$, Cre (KO) and control *Hif-2α*$^{fl/+}$, Cre mice (details supplied as supplemental information). All mice had a mixed Sv129/C57Bl6 genetic background. All animal experiments were conducted in accordance with the National Institutes of Health guidelines for use and care of live animals and were approved by the University of Pennsylvania Institutional Animal Care and Use Committee.

Whole-mount LacZ staining of embryos and histologic analyses

Mice carrying the conditional *Hif-2α*^{fl} allele were crossed to the ROSA26R reporter strain and E11.5 embryos obtained from timed matings between *Hif-2α*$^{fl/fl}$, ROSA26R/ROSA26R, and VE-cadherin-Cre transgenic mice. To assess VE-cadherin promoter activity, *Hif-2α*$^{fl/+}$, ROSA26R/$^{+}$, Cre embryos were fixed and stained for β-galactosidase activity as described.[23]

Tumor xenografts

Xenograft tumors were generated by injecting 4×10^6 Lewis lung carcinoma cells (LLC) or 1.5×10^6 B16F1/B16F10 melanoma cells subcutaneously on flanks of control and KO mice. To visualize hypoxic regions, mice were injected intraperitoneally with 150 μL of 1 mg/mL pimonidazole (Millipore) 1 hour before sacrifice. Tumors were either fixed and embedded in paraffin or frozen in optimal cutting temperature solution (Miles) for tissue sectioning. Pimonidazole and Apo-BrdU (TUNEL) apoptosis reagents were used according to manufacturer's instructions. Lungs were fixed, embedded, and serially sectioned to evaluate metastasis formation. Tumor blood vessels from control and KO mice were visualized using PECAM/CD31 antibodies for LLC tumors, smooth muscle actin (SMA) for B16F1 tumors, and S100 for B16F1/B16F10 metastases. Data were quantified as described in supplemental information.

Vascular permeability assessment

Control and KO mice were anesthetized with Avertin and tail veins injected with Evans blue dye (Sigma-Aldrich) at 50 mg/kg (0.1 mL of 0.5% solution/10 g) as described.[24] Recombinant murine VEGF or phosphate-buffered saline (PBS) vehicle control was then injected intradermally and leaked dye quantified after extraction (see supplemental information). Lung plasma protein leakage was assessed by hematoxylin and eosin (H&E) staining of lung sections.

Echocardiography, heart parameters, and pulmonary arterial pressure

Transthoracic echocardiography was performed as described[25] with minor modifications (see supplemental information). Briefly, mice were anesthetized using an integrated isoflurane-based system and electrocardiography monitored continuously using a Vevo 770 Visual Sonic machine. For pulmonary arterial (PA) measurements, a catheter transducer inserted into the right ventricle was positioned in the pulmonary artery to measure systolic PA pressure (see supplemental information). For each mouse, 2 to 4 PA measurements were analyzed, each corresponding to the average of 10 to 20 individual data points. After sacrifice, hearts were weighed to establish the heart-to-body weight ratios (n = 12 for each age group).

Confocal microscopy of tumor vasculature

Tumor-bearing mice were anesthetized with Avertin and injected with 100 μL of 1 mg/mL fluorescein isothiocyanate (FITC) tomato (*Lypersicon esculentum*) lectin (Vector Laboratories) in PBS intravenously into the tail vein, after which mice were perfused with PBS intracardially. For confocal imaging of the vasculature, tumors were excised and embedded in optimal cutting temperature compound. Frozen sections (20 μm) were fixed with 4% paraformaldehyde and mounted in Fluoromount-G media (Southern Biotech). For each tumor, 6 images obtained randomly using a Zeiss LSM 510 confocal laser-scanning microscope. The number of vessels and the vasculature area were determined as described[26] using Zeiss AIM software. Briefly, vascular area was defined as the combined area of FITC-labeled vessels plus lumens in 6 independent fields, expressed as a percentage of the total image area.

Endothelial cell isolation and characterization

Immortalized endothelial cell populations were generated from lung tissues of KO and control mice as described,[27] with minor modifications (see supplemental information). Endothelial cells used for the acute deletion experiments were generated from lung tissues of *Hif-2α*$^{fl/\Delta}$, Ubc-CreER^{T2} mice[22] (and supplemental information).

Matrigel and fibronectin adhesion assay

Adhesion assays were performed as described[28] and in supplemental information.

Quantitative real-time polymerase chain reaction analysis

Total RNA was isolated from purified endothelial cells grown under normoxic (21% O_2) conditions, or exposed to 16 hours of hypoxic (0.5% O_2), or anoxic (0% O_2) conditions, using Trizol reagent (Invitrogen). Primers for specific transcripts were designed using PrimerExpress 1.0 software (sequences listed as supplemental information). Quantitative real-time polymerase chain reaction (PCR) was performed on EC RNAs using Syber Green PCR Master Mix (Invitrogen) and the Applied Biosystems 7900HT Sequence Detection System (TaqMan). β-actin or 18S rRNA was used as endogenous control in the ΔΔCT analysis. RNA expression profiling was performed on triplicate samples of KO and control RNAs using Affymetrix gene chips according to protocols supplied by the University of Pennsylvania School of Medicine Microarray Core Facility. The microarray data have been deposited in the Gene Expression Omnibus (National Center for Biotechnology Information, http://www.ncbi.nlm.nih.gov/geo/) under accession number GSE16067.

Microscopic analysis

Micrographs were obtained using a Leitz DMRB microscope equipped with a 20×/0.60 PH2 dry objective lens. Slides were mounted using VECTASHIELD mounting medium (Vector Laboratories). Images were captured using a Leica DC500 digital camera and associated software, and processed using Adobe Photoshop 6.0 (Adobe Systems).

Statistical analysis

Results shown represent average plus or minus the standard error of the mean (SEM) of 6 to 9 samples from 2 to 3 independent studies. Statistic analyses were done using 2-tailed Student *t* test. Error bars represent SEM for all figures. A *P* value less than .05 was defined as statistically significant. A *P* value less than .01 was defined as highly significant.

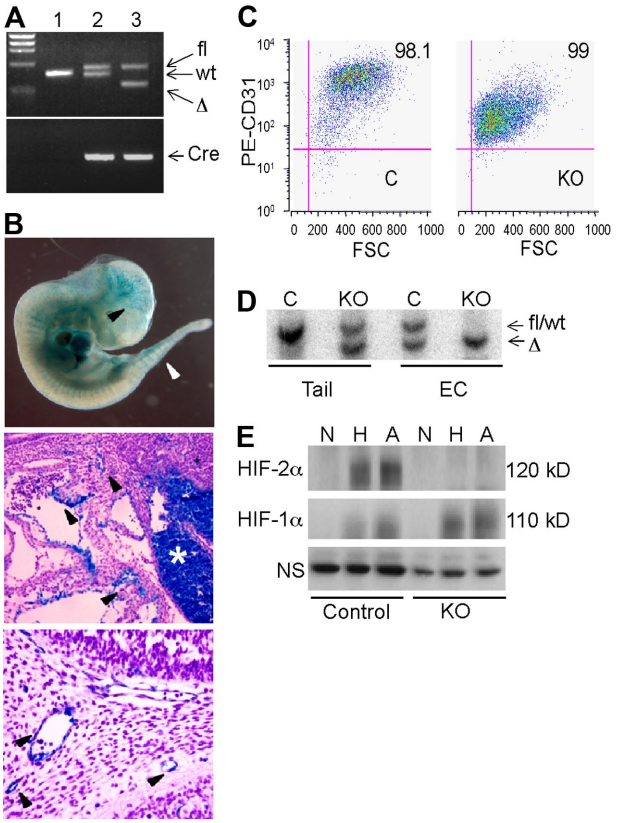

Figure 1. Characterization of an endothelial *Hif-2α* conditional allele. (A) PCR genotypes of mouse tail genomic DNA. Lane 1, wild-type; lane 2, *Hif-2α*$^{fl/+}$, *Cre* (control); lane 3, *Hif-2α*$^{fl/\Delta}$, *Cre* (KO). (B) β-galactosidase (lacZ) expression in E11.5 *Hif-2α*$^{fl/+}$, ROSA26R/$^{+}$, Cre embryos and tissue sections. Arrowheads indicate lacZ activity in ECs. Middle panel depicts vascular ECs near the hepatic primordium (*), which also contains lacZ-positive hematopoietic cells. Bottom panel depicts blood vessels in the branchial arch region. (C) Flow cytometric analysis of lung ECs isolated from control (C) and knockout (KO) mice upon staining with PE-conjugated anti-CD31 antibody. (D) Southern blot analysis of DNA from tail clips and corresponding endothelial cell (EC) populations, indicating highly efficient recombination of *fl* allele in both control (C) and knockout (KO) EC. Wild-type and *fl* alleles are not distinguishable by size. (E) Western blot analysis of HIF-1α and HIF-2α protein expression in endothelial cells subjected to 21% (N), 0.5% (H), or 0% (A) O_2 for 6 hours. The bands appear diffuse due to phosphorylation and other posttranslational modifications.[7] NS indicates nonspecific band used as a loading control.

Results

Generation of an EC-specific HIF-2α deletion murine strain

A conditional "floxed" allele of the murine *Hif-2α* genomic locus was generated by flanking the exon encoding the DNA binding bHLH domain with loxP sites[22] (supplemental Figure 1A-B). *Hif-2α*$^{fl/fl}$ mice were bred to VE-cadherin-Cre (Cre) transgenic mice[23] to obtain *Hif-2α*$^{fl/+}$, Cre (designated as control) and *Hif-2α*$^{fl/\Delta}$, Cre (designated "KO") mice (Figure 1A and supplemental Figure 1A-B). To assess VE-cadherin-Cre transgene expression in the 129 *Sv*/C57/B6 genetic background, control mice were crossed to a strain carrying the ROSA26R β-galactosidase reporter allele as previously described.[23] β-galactosidase activity in E11.5 *Hif-2α*$^{fl/+}$, ROSA26R/$^{+}$, Cre embryos was detected in brain vasculature, intersomitic vessels, dorsal aorta, and fetal liver (Figure 1B). Histologic sections revealed significant but discontinuous β-galactosidase expression in embryonic vessels (Figure 1B). These results are consistent with the original characterization of embryonic VE-cadherin-Cre transgene expression, in which the degree of vessel staining increased from E8.5-13.5 and was essentially uniform from E14.5 onward in all endothelial compartments[23] (data not shown).

To determine the endothelial-specific recombination efficiency of the *Hif-2α*^{fl} allele, primary ECs were isolated from the lungs of control and KO mice, immortalized by infection with a retrovirus expressing the polyomavirus middle T antigen, and selected with anti-CD31 antibodies. Flow cytometric analysis (Figure 1C) indicated that these populations were highly enriched for ECs, as approximately 95% of the cells expressed CD31. Once purified, these cells also stained positively for CD31 and von Willebrand factor expression by immunofluorescence and took up DiI-Ac-LDL, a characteristic of ECs (data not shown). Importantly, Southern blot analysis of genomic DNA demonstrated highly efficient recombination of the *Hif-2α*^{fl} allele in both control and KO ECs (Figure 1D). Western blot analysis of whole cell extracts revealed that HIF-1α was induced in both control and KO mice under hypoxia and anoxia, as expected. In contrast, HIF-2α proteins were detected only in control ECs (Figure 1E). Together, these studies indicated that HIF-2α is efficiently ablated in the endothelial compartment of adult KO mice.

As the VE-cadherin promoter is active in embryonic hematopoietic cells and in approximately 50% of bone marrow hematopoietic cells in adults,[23] we performed whole blood analysis of 3-month-old mice. All hematopoietic lineages were present at comparable levels in control and KO mice (supplemental Figure 1D), suggesting that any HIF-2α deletion that occurred in hematopoietic lineages did not significantly affect blood cell development and homeostasis in mice.

Endothelial HIF-2α deletion disrupts vessel integrity and promotes pulmonary hypertension

Hif-2α$^{fl/\Delta}$, Cre (KO) and *Hif-2α*$^{fl/+}$, Cre (control) mice were born in Mendelian ratios and exhibited no obvious developmental defects. Vascular structures in several organs (brain, heart, lung, spleen, liver, kidney, ovary, uterus, and testis) from control and KO mice appeared similar, as assessed by H&E staining and CD31 immunohistochemistry (data not shown). To examine vascular integrity, Evans blue dye was injected in control and KO mice, and various organs were recovered 6 hours later. Lung and adipose tissues from KO mice exhibited higher levels of dye retention than controls, indicating increased vessel permeability in these organs (Figure 2A-B). No significant differences in dye retention were observed in KO and control kidneys and livers, indicating that HIF-2α loss affects vessel permeability in an organ-specific manner. Interestingly, KO mice exhibited increased acute vascular leakage in response to VEGF stimulation compared with control mice (Figure 2C-D). This difference was observed irrespective of age (Figure 2D and supplemental Figure 2), suggesting that increased permeability is a direct consequence of HIF-2α deletion in ECs.

Histologic analysis revealed increased red blood cell (RBC) extravasation, plasma protein leakage, and lymphocyte infiltration in lungs and adipose tissues of KO mice, consistent with increased permeability of these vessels (Figure 3A-B). Ultrastructural analysis also revealed numerous plasma membrane blebs, as well as decreased association with the basal lamina, in vessels from KO lungs (Figure 3C). The compromised structural integrity of lung EC plasma membranes in KO mice may underlie the increased capillary permeability we observed, resulting in increased leakage of fluid, proteins, and RBC into the interstitium and alveoli.

Focal lymphocyte infiltration was also detected in KO lungs (Figure 3A), suggesting pulmonary inflammation may be a consequence of increased pulmonary leakage as previously described.[29]

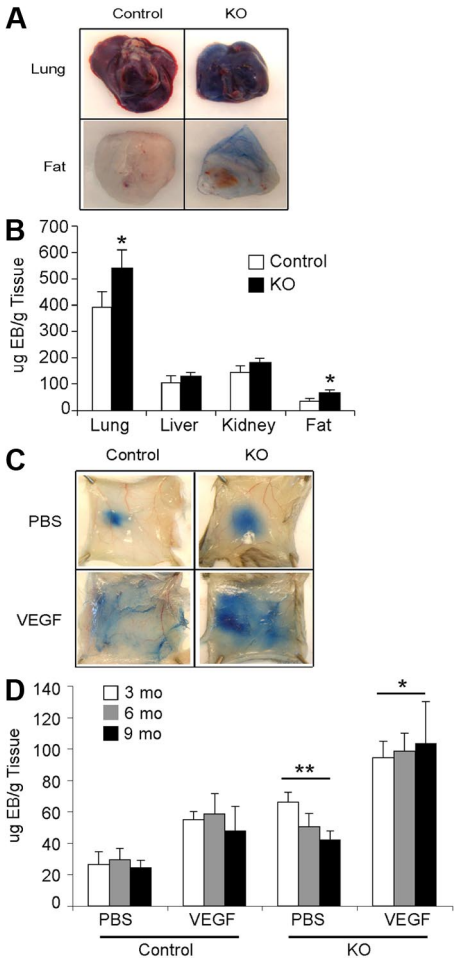

Figure 2. Effects of *Hif-2α* deletion on vessel permeability. (A) Increased vessel permeability in KO mice. Images of chronic vascular leakage in lung and adipose tissue of KO mice. (B) Quantification of Evan blue dye leakage in various organs. (C) Photographs of Evan blue dye leakage 30 minutes after intradermal injection of either PBS or VEGF into the back skin of 9-month-old control and KO mice. (D) Quantification of extracted dye from the back skin of 3-, 6-, and 9-month-old mice, normalized to tissue weight, showed significantly increased leakage in KO compared with control mice in both treatment groups (n = 8 for each age). $^{**}P < .01$; $^{*}P < .05$.

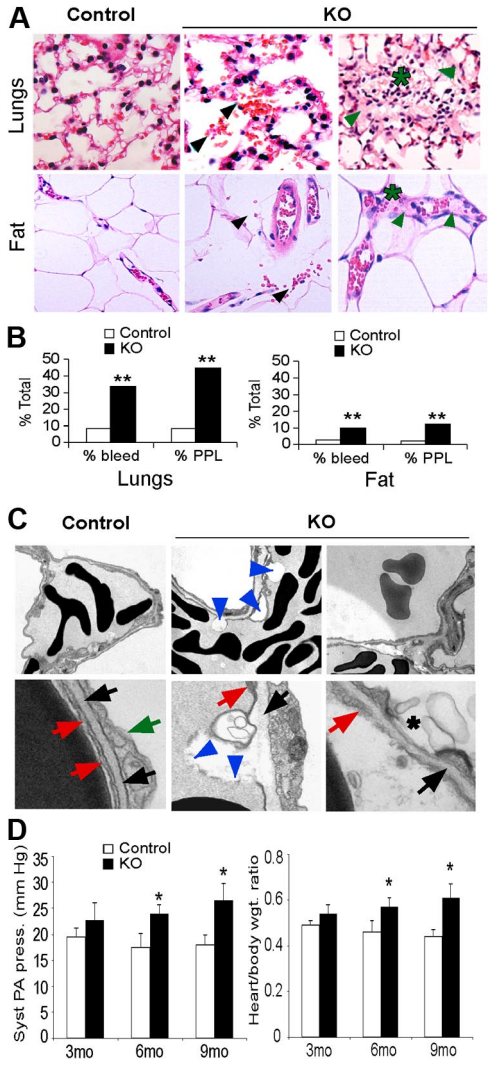

Figure 3. Hif-2α deletion affects lung endothelial cells and capillaries. (A) H&E stain of lungs and adipose tissue from control and KO mice. KO mice show increased bleeding (black arrows), plasma protein leakage (green arrows), and lymphocyte infiltration (*). Original magnification, ×200. (B) Percentage of control and KO mice that show bleeding and plasma protein leakage (PPL) in lungs and adipose tissue from 3- to 6-month-old mice; n = 6; $^{**}P < .01$. (C) Electron microscopy of lung capillaries from 6-month-old control and KO mice. Electron-dense discs are RBCs. Top row of panels show reduced EC attachment to basement membrane (blue arrowheads) and hemorrhage in KO lungs (original magnification, ×1100). Bottom row of panels show control ECs (red arrows) in contact with the basal lamina (black arrows). Green arrow, type II epithelial cell. KO ECs show areas of detachment from the basal lamina and plasma membrane discontinuity (blue arrowheads) and membrane blebs (*). Original magnification, ×11 000. (D) Systolic pulmonary arterial pressure and heart/body weight ratios reveal significant pulmonary hypertension in 6- and 9-month-old KO mice. Syst PA pressure was increased 1.5 fold in 9-month-old KO mice compared with control mice ($^{*}P < .05$). Heart-to-body ratio was also significantly increased in 6- and 9-month-old KO mice compared with the control mice (1.4-fold). $^{*}P < .05$; n = 6.

As lung edema can promote pulmonary hypertension, we analyzed pulmonary arterial pressure and cardiac hypertrophy, both of which were elevated in 3-month-old KO compared with control mice, and became more pronounced in 6- and 9-month-old mice (Figure 3D). Transthoracic echocardiography revealed a significant increase in right ventricle diameter in 6- and 9-month-old KO mice relative to control mice, as well as a modest but significant increase in right ventricle thickness in 9-month-old mice (Table 1). In contrast, left ventricle thickness and diameter were similar in mice of both genotypes. These phenotypes indicate that KO mice developed pulmonary hypertension, as systemic hypertension would be associated with hypertrophy in both ventricles.

To begin investigating the cell-autonomous basis of these phenotypes, we evaluated primary EC lines generated from lungs of KO and control mice. Consistent with our in vivo observations, KO ECs displayed reduced ability to bind to Matrigel under hypoxic conditions (Figure 4A). A similar trend was observed for EC binding to fibronectin, although statistical significance was not attained for one KO cell line (Figure 4B). It was possible that the defects we observed resulted from a long-term compensatory response, as opposed to a direct consequence of HIF-2α deletion. To address this, we analyzed the adhesive properties of ECs isolated from *Hif-2α*$^{fl/\Delta}$, Ubc-CreER^{T2} mice.[22] When these cells were exposed to tamoxifen, Cre recombinase expression and deletion of the conditional *Hif-2α* allele was induced, resulting in an acute loss of HIF-2α protein expression (Figure 4C-D). Interestingly, a similar decrease in adhesive properties was observed for these cells as for the KO cells, particularly on Matrigel (Figure 4E-F), indicating that these effects are most likely a direct consequence of HIF-2α deletion, as opposed to an indirect long-term adaptation. Finally, mRNA was prepared from KO and control ECs exposed to 0.5% O_2 and subjected to microarray analysis. Multiple transcripts encoding proteins associated with

Table 1. Cardiac characteristics for control and KO mice evaluated using echocardiography

Parameter	3 mo		6 mo		9 mo	
	Control (n = 6)	KO (n = 6)	Control (n = 6)	KO (n = 6)	Control (n = 6)	KO (n = 6)
Heart rate, bpm	462 ± 40	489 ± 65	483 ± 54	504 ± 70	530 ± 27	505 ± 39
Right ventricle characteristics						
Thickness, mm	0.23 ± 0.03	0.23 ± 0.02	0.22 ± 0.04	0.25 ± 0.07	0.28 ± 0.02	0.32 ± 0.03*
Diameter, mm	1.74 ± 0.27	1.85 ± 0.1	1.46 ± 0.09	1.79 ± 0.1*	1.73 ± 0.05	1.90 ± 0.08*
Left ventricle characteristics						
Thickness IVS, mm	0.63 ± 0.06	0.65 ± 0.06	0.65 ± 0.06	0.7 ± 0.12	0.65 ± 0.12	0.80 ± 0.07
Thickness LVPW, mm	0.74 ± 0.05	0.72 ± 0.07	0.73 ± 0.06	0.69 ± 0.13	0.86 ± 0.10	0.84 ± 0.14
LVIDd, mm	3.95 ± 0.2	4.07 ± 0.18	4.17 ± 0.14	4.3 ± 0.29	3.86 ± 0.06	4.13 ± 0.27

Data were obtained using transthoracic echocardiography and represent means ± SEM for 6 mice per group. IVS indicates intraventricular septum; LVPW, left ventricular posterior wall; and LVIDd, left ventricular diastolic dimensions.

*Statistically significant ($P < .05$) vs corresponding control mice.

cell adhesion, including ET-B, fibronectin 1 (FN1), procollagen type Vα1, and integrins α9 and β2 were decreased in hypoxic KO ECs relative to control ECs, by 6.6, 2.5, 10.3, 6.3, and 3.5×, respectively (false discovery rates < 16.7%). These results strongly suggest that the reduced expression of a cohort of genes regulating cell adhesion contribute to the vascular permeability defects observed in HIF-2α–deficient ECs.

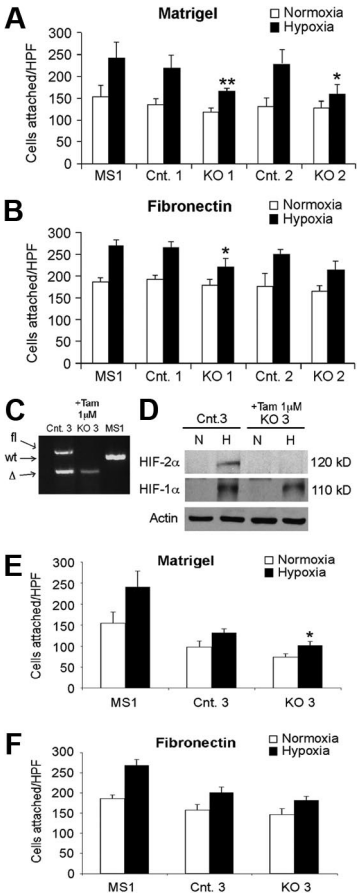

Figure 4. Hif-2α deletion affects lung endothelial cell adhesion. Reduced adhesion of independently derived KO EC lines to Matrigel- (A) or fibronectin- (B) coated plates, under hypoxic conditions, compared with related control EC lines. MS1, control murine pancreatic endothelial cell line. Cells in 6 random high power fields (HPF) were counted, and combined results from 3 separate experiments are shown. (C-D) Acute HIF-2α deletion in lung endothelial cells from *Hif-2α*$^{2L/1L}$, Ubc-CreER^{T2} mice. PCR (C) and Western blot (D) analysis demonstrating efficient deletion of HIF-2α after tamoxifen treatment. Proteins were extracted from cells after exposure to either 21% (N) or 0.5% (H) O_2 for 6 hours. (E-F) Reduced adhesion of ECs with acute HIF-2α deletion to either Matrigel- (E) or fibronectin- (F) coated plates, under hypoxic conditions, compared with related control EC lines. *$P < .05$; **$P < .01$.

HIF-2α EC null mice exhibit reduced tumor growth and angiogenesis

As multiple HIF-2α transcriptional targets regulate angiogenesis, we examined the effects of EC-specific *Hif-2α* deletion on tumor angiogenesis and growth using subcutaneous LLC xenografts. As shown in Figure 5A, the size, weight, and growth rate of tumors grown in KO mice were significantly reduced compared with those grown in control mice (Figure 5A-C). Ki67 labeling was actually increased in tumors from KO mice (Figure 5D-E), suggesting that reduced tumor growth in KO mice is not the result of altered tumor cell proliferation. Whereas tumors from both groups displayed

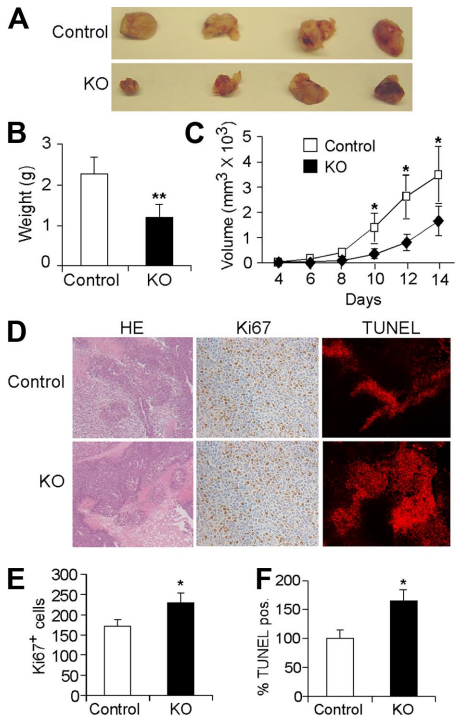

Figure 5. Endothelial *Hif-2α* deletion leads to reduced tumor growth and increased tumor cell apoptosis. (A) Representative pictures of LLC tumor xenografts from control and KO mice 14 days after subcutaneous injection (n = 9). (B) Weight of tumors excised at day 14. (C) Growth curve of LLC tumors over the 2-week course (n = 9). (D) Representative H&E staining and Ki67 and Apo-BrdU (TUNEL) immunohistochemistry. (E,F) Quantification of Ki67 and TUNEL signals in tumors isolated from control and KO mice (n = 6; * $P < .05$; ** $P < .01$).

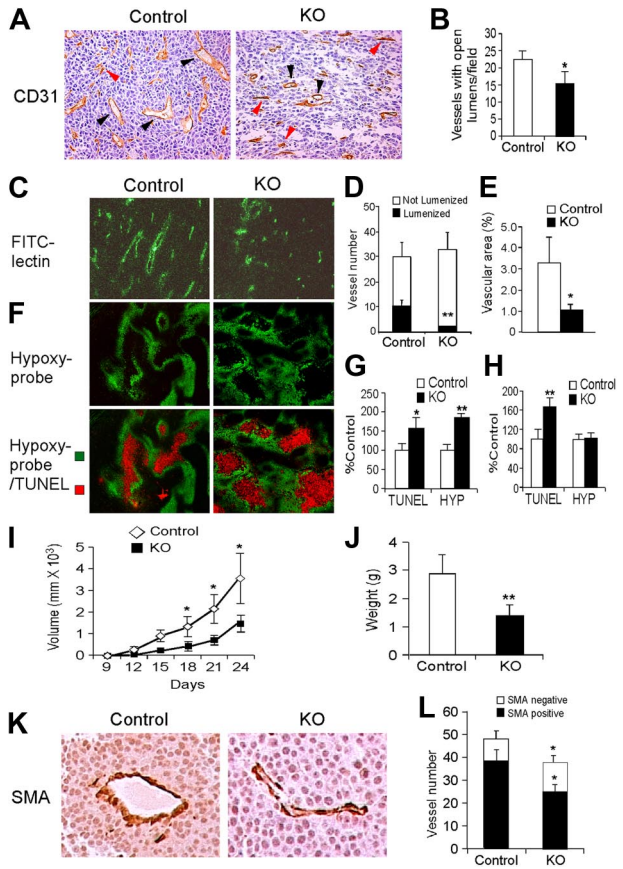

Figure 6. Effects of endothelial *Hif-2α* deletion on tumor angiogenesis. (A) Representative CD31 staining of LLC xenograft tumors, showing decreased numbers of functional vessels (black arrowheads indicate lumenized vessels, defined as vessels with open lumens) in tumors grown in KO mice. Vessels without apparent lumens are indicated by red arrowheads. (B) Quantification of number of vessels with open lumens. (C) Representative field showing FITC-labeled vessels in LLC xenografts. (D-E) Quantification of overall vessel density (total number of vessels, proportion of lumenized vessels) and vascular area. (F) Staining for hypoxia and apoptosis using pimonidazole and Apo-BrdU DNA (TUNEL) fragmentation kit. (G-H) Quantification of pimonidazole and TUNEL stains in large (> 8 mm; G) and small (< 8 mm; H) LLC xenografts. (I) Growth curves for intradermal B16F1 melanoma xenografts in control and KO mice. (J) Weight of B16F1 xenografts harvested after 28 days. (K) SMA staining of B16F1 xenografts grown in control and KO mice, showing similar mural cell coverage. (L) Vessel density, including SMA-positive and SMA-negative vessels, in B16F1 xenografts (n = 6). $^*P < .05$; $^{**}P < .01$.

regions of necrosis, TUNEL staining was significantly higher in tumors from KO mice (Figure 5D-F), demonstrating that EC-specific *Hif-2α* deletion contributes to increased tumor cell apoptosis in these xenografts.

CD31 immunostaining of tumors from KO mice revealed a significant decrease in the number of functional tumor vessels with open lumens (Figure 6A-B), which was confirmed using tail-vein injection of FITC-labeled lectin (Figure 6C). Although the density of perfused vessels in LLC tumor xenografts (Figure 6C) was not significantly different between tumors grown in control or KO mice (Figure 6D), tumors in control mice displayed larger vessels with open lumens, which correlated to increased vascular area (Figure 6B,D-E).

LLC tumor sections from mice injected with Hypoxyprobe (pimonidazole) displayed distinctive results when tumors were grouped according to size. Pimonidazole-positive hypoxic regions were significantly larger in KO tumors than control tumors in large xenografts (> 8 mm, Figure 6F-G), although not in smaller tumors (≤ 8 mm, Figure 6H). Interestingly, a significantly larger proportion of apoptotic cells were detected in KO tumors irrespective of size (Figure 6G-H). TUNEL-positive apoptotic cells were located within necrotic domains surrounded by a penumbra of hypoxic (pimonidazole-positive) cells, consistent with previous observations[30] (Figure 6F). Collectively, these results suggest that tumor vessels form at approximately equivalent numbers in KO and control mice; however, the KO tumor vessels are defective, resulting in reduced tumor growth associated with elevated tumor hypoxia and apoptosis.

In parallel experiments, we generated xenograft tumors using B16F1 and B16F10 melanoma cells, which differ in their ability to establish metastatic tumors.[31] B16F1 (low metastatic potential) or B16F10 (high metastatic potential) melanoma cells were injected subcutaneously into KO and control mice. Tumor vasculature was reduced in B16F1 KO xenografts in a manner similar to the LLC tumors, except that the reduction in vessel density reached statistical significance (Figure 6I-L). The degree of mural cell coverage in tumor vessels, as visualized by the number of associated cells expressing smooth muscle actin, was similar in melanoma xenografts grown in KO and control mice (Figure 6K-L). Finally, lung metastases from the B16F10 melanoma xenografts were identified histologically and confirmed by immunohistochemical staining for the S100 melanoma antigen (supplemental Figure 3A-B). Interestingly, fewer KO mice exhibited metastases from the highly metastatic B16F10 cells compared with the control mice (supplemental Figure 3C).

Hypoxic induction of angiogenic genes is impaired in HIF-2α–deficient ECs

To investigate the effect of EC-specific *Hif-2α* deletion on angiogenic gene expression, immortalized KO and control EC populations were exposed to 21% or 0.5% O_2, and the expression of genes known to regulate EC function and angiogenesis determined by mRNA microarray and quantitative RT-PCR analyses. Data from microarray experiments revealed that the expression of previously identified HIF-2α target genes VEGF receptor-1 (*Flt-1*) and VEGF receptor-2 (*Flk-1*) was decreased in hypoxic KO ECs relative to control ECs, by 2.3 and 1.8×, respectively (false discovery rates < 16.7%). We used quantitative RT-PCR to confirm these results and extend our analysis to include other important angiogenic genes. As shown in Figure 7A and Figure 7B, constitutive or acute deletion of HIF-2α markedly reduced hypoxic induction of genes encoding FLT-1, FLK-1, Ang2, and Dll4. We also demonstrated that HIF-2α regulates Dll4, Ang2, and FLK-1 expression in ECs using specific siRNAs (supplemental Figure 4).

Somewhat surprisingly, we observed only a modest reduction of *Vegf* mRNA in hypoxic KO cells that was not statistically significant and which probably reflects the activity of HIF-1α in HIF-2α KO ECs. Similarly, no effect of *Hif-2α* deletion on angiopoietin 1 (Ang1) mRNA levels was observed, and (as expected) hypoxic expression of the HIF-1α–specific target *Pgk* was not affected by HIF-2α deletion. Interestingly, hypoxic KO ECs expressed slightly elevated levels of endothelin-1 (ET-1) and reduced levels of ET-B mRNAs, consistent with previous observations that ET-B–deficient rats display elevated ET-1 levels, pulmonary hypertension, and increased vascular leakage and lung edema.[32] It should be noted that the fold change observed in ET-B and FN-1 expression in KO ECs by quantitative RT-PCR was somewhat reduced compared with the microarray analysis described above.

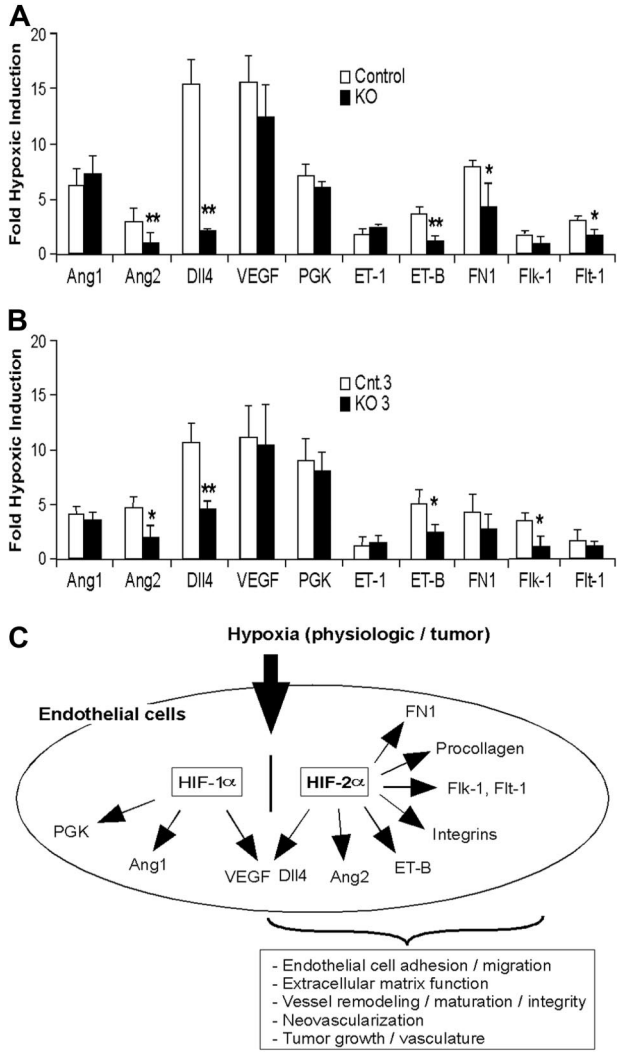

Figure 7. Hif-2α deletion affects HIF target gene expression in lung endothelial cells. (A-B) Hypoxic induction of HIF target gene expression in ECs isolated from KO mice (A) and from ECs with HIF-2α acute deletion (B) exposed to 0.5% O_2 for 16 hours. The relative ratio of hypoxic to normoxic gene expression (fold hypoxic induction) is shown for control and KO ECs. See "Endothelial HIF-2α deletion disrupts vessel integrity and promotes pulmonary hypertension" and "Hypoxic induction of angiogenic genes is impaired in HIF-2α–deficient ECs" for gene names (n = 6; $^*P < .05$; $^{**}P < .01$). (C) Model of HIF-2α function in murine ECs in response to hypoxia, reflecting unique and shared transcriptional targets of HIF-1α and HIF-2α.

Discussion

The identification of VEGF, VEGFR-1, VEGFR-2, bFGF, and other angiogenic compounds as targets of the HIF transcription factors provides a clear molecular mechanism by which hypoxic microenvironments might directly modulate angiogenesis.[1,2] Elaborating the precise roles of HIF gene family members in these processes is important, as HIF-1α and HIF-2α subunits have unique and sometimes opposing functions. For example, whereas both proteins regulate many common hypoxia-induced target genes such as VEGF,[14] HIF-1α (but not HIF-2α) activates the hypoxic expression of genes encoding glycolytic enzymes such as PGK and ALDA.[14,15] In contrast, HIF-2α uniquely regulates the gene encoding the critical stem cell factor Oct-4 in murine embryos and ES cells.[33] In addition, both HIF-1α and HIF-2α can form complexes with the c-Myc oncoprotein in multiple cell types, but whereas HIF-1α inhibits c-Myc activity,[16] HIF-2α potentiates it.[17]

The experiments presented here were designed to determine the cell-autonomous function of HIF-2α in vascular ECs. Our results demonstrate that HIF-2α deletion in murine ECs elevates VEGF-induced acute vessel permeability in 3-, 6-, and 9-month-old mice (Figure 2C-D). In addition, KO mice display increased chronic vessel permeability in selected adult organs, as well as reduced tumor angiogenesis and associated tumor cell survival. The organ specificity of vascular leakage in KO mice is interesting, as capillaries in different organs have highly variable morphology (continuous, fenestrated, and discontinuous), structural features, functions, and patterns of protein expression.[34] The increase in permeability we observed for lung and adipose tissues (continuous endothelium), but not in liver (discontinuous) or kidney (fenestrated), suggests that HIF-2α may play a specific role in continuous vascular endothelium. Future analyses of other organs bearing a continuous endothelium (brain, retina) would be of interest in this regard.

It should be noted that although the VE-cadherin Cre transgene is also active in hematopoietic cells,[23] we observed no changes in blood cells counts in *Hif-2α*$^{fl/\Delta}$, Cre (KO) mice, indicating that the effects we observed were a result of EC-specific HIF-2α deletion. This is consistent with an earlier report that defective hematopoiesis in homozygous germ line HIF-2α KO mice was not cell-autonomous and could be rescued by bone marrow transplant into wild-type recipients.[35]

As HIF-2α is strongly expressed in embryonic vascular ECs and regulates the expression of many angiogenic factors, it was initially surprising that global deletion of *Hif-2α* did not reveal profound vascular defects. The first germ line HIF-2α deletion strain reported displayed embryonic lethality around E13.5 resulting from bradycardia.[10] Interestingly, live-born mice homozygous for this *Hif-2α* mutant allele have been obtained using a complex breeding scheme but typically die postnatally with a spectrum of phenotypes associated with severe mitochondrial dysfunction.[18] In a separate genetic targeting experiment, 50% of homozygous HIF-2α–deficient embryos succumbed perinatally from acute respiratory distress.[19] In this case, decreased HIF-2α–dependent VEGF expression resulted in defective surfactant production by type II pneumocytes and a consequent block in lung maturation. Interestingly, approximately 50% of HIF-2α–deficient embryos homozygous for a third *Hif-2α* KO allele displayed yolk sac and embryonic vascular remodeling defects,[20] indicating clearly a role for HIF-2α function in angiogenesis.

The generally intact vascular system observed in our EC-specific HIF-2α KO mice strongly suggests that HIF-1α partly compensates for HIF-2α loss in ECs. This idea is consistent with reports that mice harboring an EC-specific HIF-1α deletion also develop normally but display defective adult neoangiogenesis,[36] whereas EC-specific ARNT deletion (and consequent loss of total HIF activity) resulted in substantial vascular defects associated with greater than 90% embryonic lethality.[37] Similarly, EC-specific expression of a dominant-negative HIF-α subunit that blocks both HIF-1α and HIF-2α function resulted in profound vessel defects.[38] Our observation that hypoxia-induced expression of VEGF is essentially identical in KO and control ECs indicates that either HIF-1α or HIF-2α is capable of regulating a specific subset of hypoxically induced genes in this cell type. It is also clear from the present study, however, that HIF-2α and HIF-1α are not entirely redundant, as each fulfills unique physiologic roles in ECs, particularly in the context of adult neoangiogenesis (Figure 7C). This model is supported by a previous report that HIF-2α (but not HIF-1α) cooperates with Ets-1 to control transcription of the gene encoding Flk-1 (VEGFR2) in ECs.[39]

Quantitative RT-PCR and mRNA microarray analyses of immortalized control, KO ECs, and ECs with an acute deletion of HIF-2α revealed defective hypoxic induction of target genes (Figure 7A-B) that are likely to contribute collectively to the phenotypes we observe. In particular, the reduced hypoxic expression of transcripts encoding proteins involved in adhesion and extracellular matrix formation (including procollagen type Vα1, fibronectin 1, and integrins α9 and β2) in KO ECs may explain, at least in part, their compromised adhesion characteristics in vitro. Attempts to drive expression of fibronectin 1 and/or integrins in HIF-2α KO ECs, and thereby test the specific role of these proteins in the adhesive defects, have proven unsuccessful to date as KO and control ECs are not sufficiently receptive to gene transfection.

These data also suggest a plausible model for the elevated chronic and acute vascular permeability in multiple organs of KO mice, including the lung. Defects in lung EC adhesion may lead directly to vessel leakage, which could then promote increased edema, inflammation, and pulmonary hypertension, all of which were observed in KO mice. To determine more precisely whether impaired vascular integrity in KO mice is a primary defect rather than a secondary complication to other defects such as pulmonary hypertension, we assessed vascular integrity and pulmonary blood pressure in animals of increasing age. Interestingly, increased acute vessel permeability precedes the onset of pulmonary hypertension, suggesting that defect in vasculature of the KO mice could underlie the enhanced pulmonary arterial pressure we observe. Moreover, echocardiographic results show that the cardiac hypertrophy is confined to the right ventricle with a significant increase of the thickness and the diameter, consistent with pulmonary hypertension rather than systemic hypertension, which typically affects both ventricles. These data strongly suggest that defects in the vasculature of the KO mice underlie the enhanced pulmonary arterial pressure we observe. It is also possible that HIF-2α deficiency in KO ECs causes increased hemodynamic pressure by a separate mechanism, which may result in EC detachment and pulmonary edema. In this regard, it is interesting that ET-B–deficient rats exhibit pulmonary edema and hypertension, associated with elevated endothelin-1 levels in the lung.[32] We also observed reduced ET-B expression in KO ECs, which may enhance pulmonary hypertension in KO mice in a similar manner. The elevated expression of endothelin 1 (ET-1) we observed in hypoxic KO ECs further suggests that HIF-2α can repress ET-1 in a cell-autonomous manner. These results contrast with a previously proposed role of HIF-2α in maintaining ET-1 expression in pulmonary vascular endothelial cells in vivo.[40] The reasons for this discrepancy are as yet unclear but may reflect inherent physiologic differences between mice with an EC-specific *Hif-2α* deletion and mice with global *Hif-2α* heterozygosity.[40]

LLC and melanoma xenograft tumors grew more slowly in KO than control mice and were characterized by increased hypoxia and tumor cell apoptosis. Although microvessel density was similar in both strains, tumor vessels in KO mice had reduced volume, suggesting a relative reduction in perfusion, which is consistent with the elevated hypoxia in these tumors. It is similarly intriguing that Dll4 expression is considerably reduced in KO ECs, as Dll4 is known to modulate EC functions such as adhesion, tube formation, migration or invasion.[41-45] Hypoxia, and particularly HIF-1α, have been shown to regulate Dll4 expression in several human endothelial cell lines.[45] However, the regulation of *Dll4* in ECs by both HIF-2α and HIF-1α was confirmed by transfecting specific siRNAs into murine endothelial MS1 cells and is consistent with the demonstration that the *Dll4* promoter can be activated by HIF-1α and HIF-2α in hypoxic embryonic endothelial precursor cells.[46] Interestingly, Dll4 inhibition has also been shown to promote highly branched but functionally defective tumor vessels, thereby increasing hypoxia and inhibiting tumor growth.[47,48] Finally, lung metastases from melanoma xenograft tumors were less common in KO than control mice, suggesting that EC-specific HIF-2α deletion can effectively modulate one or more aspects of the metastatic process. It is particularly intriguing that this metastatic phenotype was observed in lungs, where *Hif-2α* deletion results in structural and functional EC defects.

In summary, we used cell type–specific gene deletion to identify critical roles for HIF-2α in regulating endothelial cell function in vivo. The data reported here demonstrate that HIF-2α expression in ECs is specifically required for vessel integrity and tumor neovascularization in adult mice (Figure 7C). Our results are also consistent with a recent report in which HIF-2α was implicated in establishing a "normalized" tumor vascular bed by controlling EC survival and morphology.[49] Furthermore, these data suggest that HIF-1α and HIF-2α can partly compensate for each other in ECs during embryonic development, but each plays important and distinct roles in adult angiogenesis. Future experiments will focus on determining how specific HIF-2α targets mediate the phenotypes reported here and further work will be also required to delineate the contribution of individual HIF-2α and HIF-1α in these processes.

Acknowledgments

We thank Hongwei Yu for histologic preparations, Dr Qian-Chun Yu and Jasmine Yu for assistance with electron and confocal microscopy, and Dr Edward Morrisey and the Simon Laboratory for helpful comments.

This work was funded by the Howard Hughes Medical Institute (M.C.S.) and National Institutes of Health grant HL66130 (B.K. and M.C.S.).

Authorship

Contribution: N.S., L.L., and B.K. designed and performed research, analyzed and interpreted data, and wrote the paper; T.W., L.Y., S.P., and A.R. performed research; L.I.-A. provided mice and designed research; and M.C.S. designed research, analyzed and interpreted data, and wrote the paper.

Conflict-of-interest disclosure: The authors declare no competing financial interests.

Correspondence: M. Celeste Simon, Abramson Family Cancer Research Institute, University of Pennsylvania School of Medicine, 456 BRB II/III, 421 Curie Boulevard, Philadelphia, PA 19104-6160; e-mail: celeste2@mail.med.upenn.edu.

References

1. Carmeliet P. Angiogenesis in life, disease and medicine. *Nature.* 2005;438:932-936.
2. Coultas L, Chawengsaksophak K, Rossant J. Endothelial cells and VEGF in vascular development. *Nature.* 2005;438:937-945.
3. Pollard JW. Tumour-educated macrophages promote tumour progression and metastasis. *Nat Rev Cancer.* 2004;4:71-78.
4. Hickey MM, Simon MC. Regulation of angiogenesis by hypoxia and hypoxia-inducible factors. *Curr Top Dev Biol.* 2006;76:217-257.
5. Simon MC, Keith B. The role of oxygen availability in embryonic development and stem cell function. *Nat Rev Mol Cell Biol.* 2008;9:285-296.
6. Semenza GL. HIF-1 and human disease: one highly involved factor. *Genes Dev.* 2000;14:1983-1991.

7. Semenza GL. Hypoxia-inducible factor 1 (HIF-1) pathway. *Sci STKE.* 2007;2007:cm8.
8. Gordan JD, Simon MC. Hypoxia-inducible factors: central regulators of the tumor phenotype. *Curr Opin Genet Dev.* 2007;17:71-77.
9. Schofield CJ, Ratcliffe PJ. Oxygen sensing by HIF hydroxylases. *Nat Rev Mol Cell Biol.* 2004;5: 343-354.
10. Tian H, Hammer RE, Matsumoto AM, Russell DW, McKnight SL. The hypoxia-responsive transcription factor EPAS1 is essential for catecholamine homeostasis and protection against heart failure during embryonic development. *Genes Dev.* 1998;12:3320-3324.
11. Ema M, Taya S, Yokotani N, Sogawa K, Matsuda Y, Fujii-Kuriyama Y. A novel bHLH-PAS factor with close sequence similarity to hypoxia-inducible factor 1alpha regulates the VEGF expression and is potentially involved in lung and vascular development. *Proc Natl Acad Sci U S A.* 1997;94: 4273-4278.
12. Jain S, Maltepe E, Lu MM, Simon C, Bradfield CA. Expression of ARNT, ARNT2, HIF1alpha, HIF2alpha and Ah receptor mRNAs in the developing mouse. *Mech Dev.* 1998;73:117-123.
13. Wiesener MS, Jurgensen JS, Rosenberger C, et al. Widespread hypoxia-inducible expression of HIF-2alpha in distinct cell populations of different organs. *FASEB J.* 2003;17:271-273.
14. Hu CJ, Wang LY, Chodosh LA, Keith B, Simon MC. Differential roles of hypoxia-inducible factor 1alpha (HIF-1alpha) and HIF-2alpha in hypoxic gene regulation. *Mol Cell Biol.* 2003;23:9361-9374.
15. Raval RR, Lau KW, Tran MG, et al. Contrasting properties of hypoxia-inducible factor 1 (HIF-1) and HIF-2 in von Hippel-Lindau-associated renal cell carcinoma. *Mol Cell Biol.* 2005;25:5675-5686.
16. Koshiji M, Kageyama Y, Pete EA, Horikawa I, Barrett JC, Huang LE. HIF-1alpha induces cell cycle arrest by functionally counteracting Myc. *EMBO J.* 2004;23:1949-1956.
17. Gordan JD, Bertout JA, Hu CJ, Diehl JA, Simon MC. HIF-2alpha promotes hypoxic cell proliferation by enhancing c-myc transcriptional activity. *Cancer Cell.* 2007;11:335-347.
18. Scortegagna M, Ding K, Oktay Y, et al. Multiple organ pathology, metabolic abnormalities and impaired homeostasis of reactive oxygen species in Epas1−/− mice. *Nat Genet.* 2003;35:331-340.
19. Compernolle V, Brusselmans K, Acker T, et al. Loss of HIF-2alpha and inhibition of VEGF impair fetal lung maturation, whereas treatment with VEGF prevents fatal respiratory distress in premature mice. *Nat Med.* 2002;8:702-710.
20. Peng J, Zhang L, Drysdale L, Fong GH. The transcription factor EPAS-1/hypoxia-inducible factor 2alpha plays an important role in vascular remodeling. *Proc Natl Acad Sci U S A.* 2000;97:8386-8391.
21. Duan LJ, Zhang-Benoit Y, Fong GH. Endothelium-intrinsic requirement for Hif-2alpha during vascular development. *Circulation.* 2005;111: 2227-2232.
22. Gruber M, Hu CJ, Johnson RS, Brown EJ, Keith B, Simon MC. Acute postnatal ablation of Hif-2alpha results in anemia. *Proc Natl Acad Sci U S A.* 2007;104:2301-2306.
23. Alva JA, Zovein AC, Monvoisin A, et al. VE-Cadherin-Cre-recombinase transgenic mouse: a tool for lineage analysis and gene deletion in endothelial cells. *Dev Dyn.* 2006;235:759-767.
24. Phung TL, Ziv K, Dabydeen D, et al. Pathological angiogenesis is induced by sustained Akt signaling and inhibited by rapamycin. *Cancer Cell.* 2006;10:159-170.
25. Trivedi CM, Luo Y, Yin Z, et al. Hdac2 regulates the cardiac hypertrophic response by modulating Gsk3 beta activity. *Nat Med.* 2007;13:324-331.
26. Winter SF, Acevedo VD, Gangula RD, Freeman KW, Spencer DM, Greenberg NM. Conditional activation of FGFR1 in the prostate epithelium induces angiogenesis with concomitant differential regulation of Ang-1 and Ang-2. *Oncogene.* 2007;26:4897-4907.
27. Marelli-Berg FM, Peek E, Lidington EA, Stauss HJ, Lechler RI. Isolation of endothelial cells from murine tissue. *J Immunol Methods.* 2000;244: 205-215.
28. Jung H, Lee KP, Park SJ, et al. TMPRSS4 promotes invasion, migration and metastasis of human tumor cells by facilitating an epithelial-mesenchymal transition. *Oncogene.* 2008;27:2635-2647.
29. Peng X, Hassoun PM, Sammani S, et al. Protective effects of sphingosine 1-phosphate in murine endotoxin-induced inflammatory lung injury. *Am J Respir Crit Care Med.* 2004;169:1245-1251.
30. Leek RD, Landers RJ, Harris AL, Lewis CE. Necrosis correlates with high vascular density and focal macrophage infiltration in invasive carcinoma of the breast. *Br J Cancer.* 1999;79:991-995.
31. Fidler IJ. Selection of successive tumour lines for metastasis. *Nat New Biol.* 1973;242:148-149.
32. Carpenter T, Schomberg S, Steudel W, et al. Endothelin B receptor deficiency predisposes to pulmonary edema formation via increased lung vascular endothelial cell growth factor expression. *Circ Res.* 2003;93:456-463.
33. Covello KL, Kehler J, Yu H, et al. HIF-2alpha regulates Oct-4: effects of hypoxia on stem cell function, embryonic development, and tumor growth. *Genes Dev.* 2006;20:557-570.
34. Pasqualini R, Arap W, McDonald DM. Probing the structural and molecular diversity of tumor vasculature. *Trends Mol Med.* 2002;8:563-571.
35. Scortegagna M, Morris MA, Oktay Y, Bennett M, Garcia JA. The HIF family member EPAS1/HIF-2alpha is required for normal hematopoiesis in mice. *Blood.* 2003;102:1634-1640.
36. Tang N, Wang L, Esko J, et al. Loss of HIF-1alpha in endothelial cells disrupts a hypoxia-driven VEGF autocrine loop necessary for tumorigenesis. *Cancer Cell.* 2004;6:485-495.
37. Yim SH, Shah Y, Tomita S, et al. Disruption of the Arnt gene in endothelial cells causes hepatic vascular defects and partial embryonic lethality in mice. *Hepatology.* 2006;44:550-560.
38. Licht AH, Muller-Holtkamp F, Flamme I, Breier G. Inhibition of hypoxia-inducible factor activity in endothelial cells disrupts embryonic cardiovascular development. *Blood.* 2006;107:584-590.
39. Elvert G, Kappel A, Heidenreich R, et al. Cooperative interaction of hypoxia-inducible factor-2alpha (HIF-2alpha) and Ets-1 in the transcriptional activation of vascular endothelial growth factor receptor-2 (Flk-1). *J Biol Chem.* 2003;278:7520-7530.
40. Semenza GL. O2-regulated gene expression: transcriptional control of cardiorespiratory physiology by HIF-1. *J Appl Physiol.* 96:1173-1177, 2004; discussion 1170-1172.
41. Hodkinson PS, Elliott PA, Lad Y, et al. Mammalian NOTCH-1 activates beta1 integrins via the small GTPase R-Ras. *J Biol Chem.* 2007;282:28991-29001.
42. Scehnet JS, Jiang W, Kumar SR, et al. Inhibition of Dll4-mediated signaling induces proliferation of immature vessels and results in poor tissue perfusion. *Blood.* 2007;109:4753-4760.
43. Williams CK, Segarra M, Sierra Mde L, Sainson RC, Tosato G, Harris AL. Regulation of CXCR4 by the Notch ligand delta-like 4 in endothelial cells. *Cancer Res.* 2008;68:1889-1895.
44. Trindade A, Kumar SR, Scehnet JS, et al. Overexpression of delta-like 4 induces arterialization and attenuates vessel formation in developing mouse embryos. *Blood.* 2008;112:1720-1729.
45. Patel NS, Li JL, Generali D, Poulsom R, Cranston DW, Harris AL. Up-regulation of delta-like 4 ligand in human tumor vasculature and the role of basal expression in endothelial cell function. *Cancer Res.* 2005;65:8690-8697.
46. Diez H, Fischer A, Winkler A, et al. Hypoxia-mediated activation of Dll4-Notch-Hey2 signaling in endothelial progenitor cells and adoption of arterial cell fate. *Exp Cell Res.* 2007;313:1-9.
47. Thurston G, Noguera-Troise I, Yancopoulos GD. The Delta paradox: DLL4 blockade leads to more tumour vessels but less tumour growth. *Nat Rev Cancer.* 2007;7:327-331.
48. Noguera-Troise I, Daly C, Papadopoulos NJ, et al. Blockade of Dll4 inhibits tumour growth by promoting non-productive angiogenesis. *Nature.* 2006;444:1032-1037.
49. Mazzone M, Dettori D, Leite de Oliveira R, et al. Heterozygous deficiency of PHD2 restores tumor oxygenation and inhibits metastasis via endothelial normalization. *Cell.* 2009;136:839-851.